*The AAPS Journal (2019) 21: 82*
DOI: 10.1208/s12248-019-0352-8

*Research Article*

# Determination of IL-23 Pharmacokinetics by Highly Sensitive Accelerator Mass Spectrometry and Subsequent Modeling to Project IL-23 Suppression in Psoriasis Patients Treated with Anti-IL-23 Antibodies

**Ting-Ting Zhang,[1] Junli Ma,[2] Kenneth R. Durbin,[3] Timothy Montavon,[4] Susan E. Lacy,[5] Gary J. Jenkins,[2] Stella Doktor,[2] and J. Cory Kalvass[2,6]**

*Received 28 December 2018; accepted 10 June 2019; published online 27 June 2019*

***Abstract.*** The pro-inflammatory cytokine interleukin (IL)-23 is a key modulator of the immune response, making it an attractive target for the treatment of autoimmune disease. Correspondingly, several monoclonal antibodies against IL-23 are either in development or approved for autoimmune indications such as psoriasis. Despite being a clinical validated target, IL-23 pharmacokinetics (e.g., IL-23 synthesis and elimination rates) and the degree of target suppression (i.e., decrease in free "active" IL-23) associated with clinical efficacy are not well understood, primarily due to its ultra-low circulating levels and the lack of sensitive and accurate measurement methods. In the current work, this issue was overcome by using accelerator mass spectrometry (AMS) to measure the concentration and pharmacokinetics of human recombinant [$^{14}$C]-IL-23 following an intravenous trace-dose in cynomolgus monkeys. IL-23 pharmacokinetic parameters along with clinical drug exposure and IL-23 binding affinities from four different anti-IL-23 antibodies (ustekinumab, tildrakizumab, guselkumab, and risankizumab) were used to build a pharmacokinetics/pharmacodynamics (PK/PD) model to assess the time course of free IL-23 over one year in psoriasis patients following different dosing regimens. The predicted rank order of reduction of free IL-23 was consistent with their reported rank order of Psoriasis Area and Severity Index (PASI) 100 scores in clinical efficacy trials (ustekinumab < tildrakizumab < guselkumab < risankizumab), thus demonstrating the utility of highly sensitive AMS for determining target pharmacokinetics to inform PK/PD modeling and assessing target suppression associated with clinical efficacy.

**KEY WORDS:** IL-23; AMS; clearance; psoriasis; model.

## INTRODUCTION

Cytokines are critical modulators of immune responses and tissue homeostasis, and are targeted for the treatment of autoimmune diseases, cancer, stroke, and renal diseases (1–3). Clinically validated targets include tumor necrosis factor-α (TNF-α), IL-1, IL-6, IL-17, IL-23, and transforming growth factor-β (TGF-β) (4). Despite the clinical success of both small molecule drugs and therapeutic antibodies targeting these cytokines, *in vivo* kinetic information (e.g., clearance and synthesis rate) of these cytokines are largely unknown. The absence of this data is primarily due to the ultra-low endogenous levels of most cytokines in healthy subjects and the lack of sensitive and accurate methods to measure the levels of these proteins *in vivo* (5,6). For these reasons, it is also challenging to quantify the levels of target suppression (i.e., decrease in the free "active" form of target) with cytokine-neutralizing agents (7). The lack of kinetic values for various cytokines has hampered efforts to develop pharmacokinetics/pharmacodynamics (PK/PD) models for the suppression of cytokine activity (8,9).

Despite these difficulties, some limited PK information has been reported for therapeutic recombinant human IL-21, IL-10, IL-12, TNF-α, and IL-2 dosed in humans (10–15) and recombinant human IL-2, IL-1β, and IL-6 dosed in rats (16–18). However, these studies were done either in rodents and/or at doses significantly higher than endogenous cytokine levels. Therefore, the results may not represent the true kinetics of endogenous cytokines due to species differences or saturation of clearance mechanisms. Conversely, the work reported herein utilized the accelerator mass spectrometry (AMS) to accurately quantify the clearance of radiolabeled

[1] DMPK, Takeda Pharmaceuticals International Co., Cambridge, Massachusetts, USA.
[2] DMPK-BA, AbbVie, Inc., North Chicago, Illinois, USA.
[3] Proteinaceous, Inc., Evanston, Illinois, USA.
[4] Process R&D, AbbVie, Inc., North Chicago, Illinois, USA.
[5] Immuno-oncology, AbbVie, Inc., Redwood City, California, USA.
[6] To whom correspondence should be addressed. (e–mail: j.kalvass@abbvie.com)

IL-23 dosed at amounts comparable with that of *in vivo* expression levels.

AMS, which is capable of achieving attomolar sensitivity for [$^{14}$C] detection, was selected to measure the ultra-low (~pg/mL) levels of human IL-23 in serum. Since AMS measures the [$^{14}$C]:[$^{12}$C] ratio derived from all sources of carbon in the sample, the targeted cytokine needs to be radiolabeled with [$^{14}$C] to provide an analyte with a unique detectable signal apart from the endogenous proteins. An example of utilizing this technique to measure protein concentrations at near endogenous levels involved a phase 0 microdosing trial with human recombinant placental alkaline phosphatase (19).

IL-23 was subjected to this analysis given its prominence as a clinical target and due to the lack of published data describing its endogenous synthesis and degradation kinetics in human.

IL-23 belongs to the IL-6/IL-12 cytokine family and is a heterodimer composed of p19 and p40 subunits (20). The p19 subunit is unique to this cytokine and exclusively binds to the IL-23R subunit of the IL-23 receptor, while p40 is a shared subunit with IL-12 and binds to a shared receptor subunit IL-12Rβ1 (21,22). IL-23 is produced by different cell types, including monocytes, macrophages, neutrophils, myeloid dendritic cells, endothelial cells, and keratinocytes in response to microbial infection and pro-inflammatory cytokines (23–27). IL-23 induces the differentiation of naive CD4 T cells into TH17 cells (28). In addition, other innate immune cells responsive to IL-23 are termed as "type 17" cells which contain the retinoic acid receptor-related orphan receptor-gt (RORgt) (29). Both TH17 and type 17 cells stimulate the production of pro-inflammatory cytokines, including IL-17, IL-22, TNF-α, and granulocyte-macrophage colony-stimulating factor (GMCSF), which recruit inflammatory immune cells and result in undesired chronic inflammation in autoimmune conditions (30–33).

As IL-23 plays a central role in both innate and adaptive immunity, it has been targeted to treat several diseases, including psoriasis, psoriatic arthritis (PsA), inflammatory bowel disease (IBD), multiple sclerosis (MS), and asthma (32,34,35). Ustekinumab, an anti-p40 subunit human monoclonal antibody (mAb), has been approved by the US Food and Drug Administration (FDA) to treat Crohn's disease, moderate-to-severe plaque psoriasis, and PsA. Guselkumab and tildrakizumab, which target the p19 subunit of IL-23, are approved for the treatment of moderate-to-severe plaque psoriasis in adults. Another anti-p19 mAb, risankizumab, has exhibited efficacy and safety in the treatment of moderate-to-severe chronic plaque psoriasis in phase 3 trials. Differential clinical efficacies and dosing regimens among the agents drove our interest in measuring IL-23 pharmacokinetics and developing a PK/PD model with these values to assess the suppression of IL-23 upon treatment with anti-IL23 drugs in psoriasis patients.

In this study, [$^{14}$C]-labeled human recombinant IL-23 was administrated to cynomolgus monkeys, which express IL-23 exhibiting 98% homology to the human protein. The disappearance of [$^{14}$C]-IL-23 was quantified using AMS detection. IL-23 clearance and volume of distribution were calculated and applied in a mathematical model derived from a basic target-mediated disposition model for biologics (36,37). Suppression of IL-23 was predicted for the dosing regimens of four different anti-IL-23 antibodies (ustekinumab, tildrakizumab, guselkumab, and risankizumab) and compared with the observed efficacy of these mAbs from clinical trials in psoriasis.

To our knowledge, this is the first-time human IL-23 clearance, volume of distribution, and half-life were measured in monkeys. This information enabled the development of a PK/PD model to assess the time-course of free "active" IL-23 in psoriasis patients following different dosing regimens of IL-23 antibodies and the comparison with reported clinical efficacies. Overall, these results suggest that the strategy reported herein could be used to measure the clearance of other soluble proteins that are therapeutic targets and define likely efficacious doses of antibody drug candidates at early stages of drug development.

## MATERIALS AND METHODS

### Materials

Human recombinant IL-23 was obtained from eBiosciences (Thermo Fisher, cat# 34-8239-82 Grand Island, NY) and stored at − 80°C prior to use. Aqueous solutions of reagents were prepared using water for injection (WFI, GE Healthcare Life Sciences, Logan, UT). Aqueous [$^{14}$C]-formaldehyde (specific activity of 55 mCi/mmol) was purchased from American Radiolabeled Chemicals, Inc. (St. Louis, MO). Purification of [$^{14}$C]-formaldehyde was accomplished by centrifugal filtration over a bed of Amberlyst A-21 free base using a Sartorius Vivaspin 500 centrifugal concentrator (10,000 Da MWCO). The radiochemical purity of purified [$^{14}$C]-formaldehyde was confirmed to be > 96% by conversion to the corresponding 2,4-dinitrophenylhydrazone and subsequent HPLC analysis (38). All other reagents and chemicals, including borane dimethylamine (BDMA), were purchased from Sigma Aldrich (St. Louis, MO).

Reactions were performed in Nunc ™ sterile 15 mL polypropylene conical centrifuge tubes (Thermo Scientific, Rochester NY, cat# 339651). Desalting of reaction mixtures was performed using PD-10 Sephadex G-25 M columns (GE Healthcare Life Sciences, Buckinghamshire, UK). Diafiltration was performed using Vivaspin 6 centrifugal concentrators (30 kDa MWCO, GE Healthcare Life Sciences, Buckinghamshire, UK). Scintillation counting was performed on a PerkinElmer Tri-Carb 2800TR liquid scintillation counter (LSC) using Instagel Plus Universal LSC cocktail for sample preparation.

Prior to the preparation of dosing solutions, protein samples were stored in 1.5 mL Protein LoBind tubes (Hamburg, Germany). Dosing solutions were prepared in 30-mL sterile glass vials (Hospira, Lake Forest, IL).

### Methods

#### *Radiolabeling of Recombinant IL-23*

[$^{14}$C]-IL-23 was prepared via reductive methylation of free lysine residues using [$^{14}$C]-formaldehyde. The pH of the purified [$^{14}$C]-formaldehyde solution was adjusted to 7.5 by

addition of 0.1 N NaOH (Fisher Scientific, Fair Lawn, NJ), providing a 0.90 μCi/μL final solution. Solutions of 1.0 M BDMA and glycine were prepared immediately prior to use using water for injection and PBS buffer (pH 7.4, Gibco-Life Technologies, Grand Island, NY), respectively.

An aliquot (1.0 mL) of a 0.5 mg/mL solution of human recombinant IL-23 was adjusted to pH 6.9 with 0.1 N NaOH and the solution was cooled to 8°C. Twice, BDMA (1.54 μL) and [$^{14}$C]-formaldehyde (0.187 mL, 3.1 μmol) were added and the reaction was allowed to proceed for 3 h. Additional BDMA (0.77 μL) was added and the reaction was allowed to progress overnight. A portion of the reaction mixture was analyzed by size-exclusion chromatography (SEC) with radio-flow detection. Since the desired level of conversion was not reached, additional BDMA (0.77 μL) and [$^{14}$C]-formaldehyde (0.094 mL, 1.55 μmol) were added and the reaction was allowed to progress for 2 h at room temperature. BDMA (0.5 μL) was added to quench any unreacted formaldehyde and the mixture was incubated for 1.5 h.

The mixture was cooled to 8°C, glycine (9.6 μL, 9.6 μmol) was added, and the mixture was incubated for 45 min. The crude product was desalted over a PD-10 Sephadex G-25 M column pre-equilibrated with pH 7.4 PBS buffer. Three additional cycles of buffer exchange/concentration were performed by diafiltration providing 10.05 μCi of the labeled protein in 0.91 mL of solution. The concentration of the protein (0.472 mg/mL) was determined by a Bradford BCA assay. Endotoxin levels were determined to be 4.17 EU/mL on an Endosafe portable test system (Charles River Laboratories, Charleston, SC) using PTS20F Limulus amebocyte test cartridges (Charles River Laboratories, Charleston, SC).

SEC analysis was performed on an Agilent 1100 Series HPLC with an in line IN US Beta-Ram Model 4 Radio HPLC detector equipped with a 500 μL flow cell. The analysis was performed using isocratic elution on a Waters Acquity UPLC BEH SEC column (125 Å, 1.7 μm, 4.6 × 150 mm) equipped with a Waters Acquity UPLC Protein BEH SEC guard column (200 Å, 1.7 μm, 4.6 mm × 30 mm). Elution was performed at 25°C with a flow rate of 0.25 mL/min using a 90:10 mixture of pH 7.0100 mM phosphate buffer containing 100 mM NaCl and acetonitrile. A wavelength of 280 nm was used for detection. Radiochromatograms were recorded using Flow Logic HA liquid scintillation fluid (LabLogic).

### *Characterization of [$^{14}$C]-IL-23 Bioactivity*

The bioactivity of IL-23 was characterized using a HeLa STAT 3 luciferase reporter cell line (Signosis, Santa Clara CA, cat# SL-0003) expressing IL-23R. Briefly, cells were transiently co-transfected with a CMV promoter-driven plasmid expressing the human IL-12Rβ1 subunit and an EF6 promoter-driven plasmid expressing the human IL-23Rα subunit. Forty-eight hours post-transfection, the cells were incubated with IL-23. Serial dilutions of [$^{14}$C]-IL-23 and native IL-23 were prepared in a sterile 96-well assay block ranging from 0.02 to 334 ng/mL across 11 concentrations. A total of 50 μL aliquots of diluted solutions were dispensed to a 96-well TC plate (Perkin Elmer, Waltham, MA, cat# 6005181) and 50 μL of transiently transfected cells were then added to each well (500 cells/μL or 25 K/well). After an overnight incubation at 37°C, 5% CO2, the cell plate was allowed to cool to room temperature and 100 μL of Promega Steady Glo (Promega, Madison, WI, cat# E2520) prepared according to the manufacturer's directions was added to each well. After gently shaking the plate in the dark for approximately 5 min to lyse the cells, the plate was read for luminescence on a plate reader.

### *Intravenous Dosing of [$^{14}$C]-IL-23 in Cynomolgus Monkey*

The *in vivo* studies with cynomolgus monkeys were carried out at AbbVie Inc., North Chicago, IL, in full compliance with local, national, ethical, and regulatory principles and local licensing regulations, per the spirit of Association for Assessment and Accreditation of Laboratory Animal Care (AAALAC) expectations for animal care and use/ethics. Three female cynomolgus monkeys were administrated intravenously with [$^{14}$C]-IL-23 at a target dose of 200 ng/2 mL/animal in PBS (pH 7.4). Blood samples were collected from each monkey at pre-dose and at 0.25, 1, 2, 3, 4, 6, 8, 10, 24, 32, and 48 h post-dose. After clotting, serum samples were collected, aliquoted, and stored at − 80°C prior to processing.

### *Affinity Purification*

To enrich the specific [$^{14}$C]-IL-23 signal from endogenous [$^{14}$C] background levels, monkey serum samples were subjected to an immunoaffinity enrichment step prior to AMS analysis. Briefly, samples containing 1.5 mL of monkey serum were incubated with 150 μL of biotinylated anti-human IL-12/IL-23 p40 mouse IgG (Thermo Fisher "eBioscience," Grand Island, NY, cat# 13-7129) for 3 h at room temperature with rotation. The mixture of antibody and serum was then incubated overnight with magnetic streptavidin Dynabeads (Thermo Fisher "Invitrogen," Grand Island, NY) at 4°C with rotation. The beads were washed with 1.5 mL 1X PBS once, followed by one wash with 1.5 mL water. Protein was eluted from the beads with 0.1 M glycine solution at pH 2.0. For western blot analysis, proteins separated on a 1.0 mm 4–12% NuPAGE gel were transferred to a PDVF membrane, and an anti-IL-12/23 p40 polyclonal antibody (2 μg/mL, R&D Systems, Minneapolis, MN, cat# AF309) was used as the primary antibody to detect IL-23. The primary mAb was detected by Alexa Fluor 800 donkey-anti-goat IgG (H&L) (1:10000 dilution, Rockland Immunochemicals, Limerick, PA, cat# 605-732-125). An odyssey Fc Infrared Imaging System (LiCor Biosciences) was used to scan and quantitate bands on the western blots.

### *[$^{14}$C]-IL-23 Loss Due to Non-specific Binding Under Storage and Dosing Conditions*

A 10 μg/mL solution of [$^{14}$C]-IL-23 was prepared in a 1.5 mL Protein-Low Bind Eppendorf tube by dilution of an aliquot of a 0.47 mg/mL solution of [$^{14}$C]-IL-23 (4.2 μL) with pH 7.4 PBS buffer (195.8 μL). The solution was assayed by LSC in duplicate as follows: an aliquot (10.0 μL) was diluted with dimethylformamide (DMF) (1.0 mL), 15 mL of scintillation cocktail was added, and the samples were counted.

Separately, two 100 ng/mL mock dosing solutions were prepared in 30 mL sterile glass vials by addition of an aliquot

of a 10 μg/mL solution of human IL-23 (100 μL) to pH 7.4 PBS buffer (9.9 mL). Immediately after dilution, each solution was assayed in duplicate by LSC as follows: aliquots (100 μL each) were diluted with DMF (1.0 mL), 15 mL of scintillation cocktail was added, and the samples were counted. Bottled solutions were stored at 4°C for 18 h and were assayed by LSC as above.

The bottled solutions were warmed to room temperature and three aliquots (2.4 mL each) of each solution were taken up in separate 23-g syringe/butterfly assemblies (3/4 in. needle and 12 in. tubing). A portion (0.4 mL) of each sample was voided and the remaining samples were collected in 1.5 mL Protein-Low Bind Eppendorf tubes. Each sample was analyzed by LSC as follows: aliquots (0.75 mL each) were diluted with DMF (1.0 mL), 15 mL of scintillation cocktail was added, and the samples were counted.

### *Accelerator Mass Spectrometry Analysis of Monkey Serum Samples*

IL-23 levels in monkey serum samples were measured using AMS at Xceleron Inc. (Germantown, MD). The AMS results are expressed as Percent Modern Carbon (pMC), where 100 pMC is equal to 13.56 dpm/g C. In order to obtain a value for drug-related [$^{14}$C], standard curve samples were prepared at 0.05, 0.1, 0.5, 1, 5, 10, 50, 100, 500, and 1000 pg/mL via spiking of [$^{14}$C]-IL-23 in monkey serum. Standard samples were processed identically to PK samples. The background level of [$^{14}$C] existing in glycine buffer and untreated cynomolgus serum samples were analyzed by AMS and used for background subtraction. Monkey serum samples after immunoaffinity purification were analyzed. The LLOQ was determined as 0.22 pg/mL.

### *Antibody/Ligand Kinetic PK/PD Model for Free IL-23 Suppression*

The PK/PD model for IL-23 ligand suppression is shown in Fig. 1. Briefly, a compartmental PK model was used to simulate targeted drug exposure. The percentage of drug-bound and free IL-23 compared with the initial baseline was predicted using a model derived from a modified version of the target-mediated drug disposition model (36). A quasi-equilibrium (QE) model with affinity constant $K_D$ replacing $k_{on}$ and $k_{off}$ was used in this work (39).

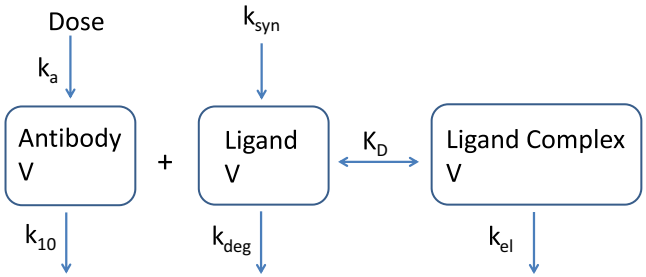


**Fig. 1.** Diagram of ligand-antibody-binding model $k_a$ and $k_{10}$ are the absorption and elimination rates of antibody drug. $k_{syn}$ and $k_{deg}$ are synthesis and degradation rates of the ligand. $K_D$ is the affinity of an antibody to the ligand. $k_{el}$ is the elimination rate of the antibody and ligand complex. $V$ is the volume of distribution of ligand

The equations in the model used in the current work are:

$$dAa/dt = -Aa \times ka \tag{1}$$

$$\frac{dCtot}{dt} = Aa \times \frac{ka}{V} - k10 \times C1 - Ctot \times kel + kel \times C1 \tag{2}$$

$$\frac{dRtot}{dt} = ksyn - (kel - kdeg) \times (Ctot - C1) - (kdeg \times Rtot) \tag{3}$$

$$C1 = 0.5 \times \left( Ctot - Rtot - KD + \sqrt{(Ctot - Rtot - KD)^2 + 4 \times KD \times Ctot} \right) \tag{4}$$

$$Initial\ Rtot = ksyn/kdeg \tag{5}$$

One compartmental model following a subcutaneous (SC) dosing was used to describe the pharmacokinetics of four anti-IL23 mAbs (ustekinumab, tildrakizumab, guselkumab, and risankizumab). In the above equations, $C_1$ is the unbound concentration of the drug. $R_{tot}$ is the total concentration of unbound and bound cytokine IL-23. $C_{tot}$ is the sum of the total concentration of the drug (bound and non-bound). $k_a$ and $k_{10}$ are the absorption and elimination rates of anti-IL23 mAbs. $k_{syn}$ and $k_{deg}$ are synthesis and degradation rates of IL-23. $k_{deg}$ was calculated by dividing IL-23 clearance (3.32 L/h, allometrically scaled) by its volume of distribution (20 L). $k_{syn}$ was estimated from the product of IL-23 baseline $C_{ss}$ (100 pg/mL; 0.00189 nM) and $k_{deg}$. $K_D$ is the affinity of the drug to IL-23. $k_{el}$ is the elimination rate of anti-IL23 mAb and IL-23 complex which is assumed to be the same as $k_{10}$ of corresponding antibodies (40).

The IL-23 ligand-binding model was established in Phoenix WinNonlin Version 6.3 (Pharsight Corporation, Mountain View, CA) with a user-defined model.

### *Pharmacokinetics Analysis*

Pharmacokinetic parameters for IL-23 were calculated with Phoenix WinNonlin Version 6.3 (Pharsight Corporation, Mountain View, CA) by a non-compartmental analysis (Model 200-202) and the linear trapezoidal method.

## RESULTS

### Radiolabeling and Characterization of [$^{14}$C]-IL-23

The specific activity of the labeled IL-23 was 1249 mCi/mmol. An average of twenty-three [$^{14}$C]-methyl groups were added to the twenty-nine lysine residues in IL-23 (Fig. 2a–c). Characterization of radiolabeled IL-23 using size-exclusion chromatography (SEC) indicated that, similar to native unlabeled IL-23, the monomeric form of the protein was the predominant analyte. Levels of aggregation were elevated to 31% from 18% for the native unlabeled IL-23 stock, indicating that the lysine-labeling procedure led to an increase in aggregation (Fig. 2d). Consequently, the

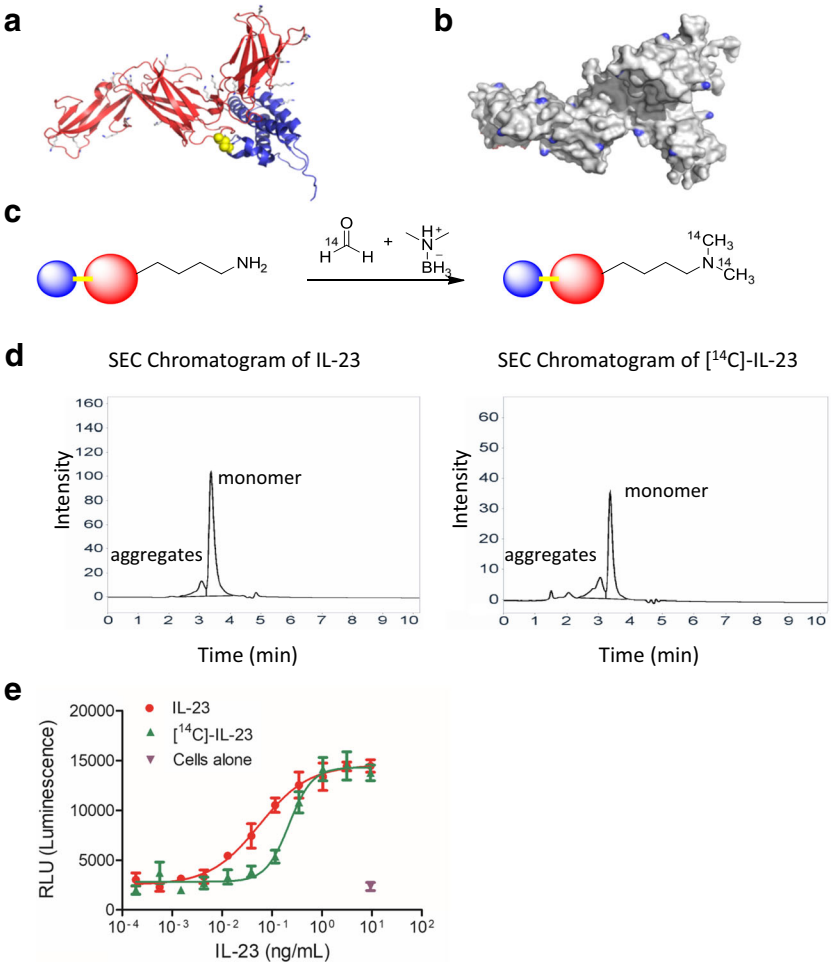


**Fig. 2.** Structure, synthesis, and characterization of [$^{14}$C]-IL-23. **a** Ribbon diagram of human IL-23 (PBD code: 3DUH (41)). The p40 subunit is colored red, the p19 subunit is colored blue, disulfide bonds are shown as yellow spheres, and lysine residues are shown as sticks. **b** Surface representation of IL-23 with lysine residues colored blue. **c** Reductive methylation of IL-23 with [$^{14}$C]-formaldehyde. **d** SEC analysis of native and [$^{14}$C]-IL-23. **e** IL-23 bioactivity analysis in human IL-23R-expressing HeLa STAT3 luciferase reporter cells

bioactivity of [$^{14}$C]-IL-23 was tested to ensure its activity was not significantly modified as a result of radiolabeling.

The bioactivity of [$^{14}$C]-IL-23 was determined using a human IL-23R-expressing HeLa STAT3 luciferase assay. [$^{14}$C]-IL-23 showed similar but slightly higher $EC_{50}$ (11.7 ng/mL *vs* 3.0 ng/mL for native IL-23) (Fig. 2e).

## Immunoaffinity Enrichment and Non-specific Binding Evaluation

The kinetics of the human IL-23 were measured by intravenously dosing [$^{14}$C]-labeled human IL-23 to cynomolgus monkeys, which is highly homologous (97.7% for p40 subunit, 98.2% for p19 subunit) to human. Since preliminary AMS measurements indicated much lower serum concentrations than were expected, monkey serum samples were subjected to an immunoaffinity enrichment step prior to AMS analysis to enrich the specific [$^{14}$C]-IL-23 signal from endogenous [$^{14}$C] background levels. The recovery of [$^{14}$C]-IL-23 was initially assessed by western blot analysis at high nanogram levels of [$^{14}$C]-IL-23. Compared with control samples where [$^{14}$C]-IL-23 was directly spiked into the loading buffer used for western blots, signals from samples which were spiked in serum and went through affinity purification were lower, indicating the loss of [$^{14}$C]-IL-23 during this purification step (Fig. 3a). A standard curve was prepared with spiked samples and was processed identically to PK samples to calibrate this loss.

Additionally, the loss of [$^{14}$C]-IL-23 in dosing solution during storage and administration was assessed by replicating the dosing conditions used in the monkey study. [$^{14}$C]-IL-23 concentration decreased to 38% of the original amount following overnight storage. The concentration was reduced further to 7.6% of the original after injecting mock IL-23 dose solutions through butterfly catheters (Fig. 3b), suggesting strong non-specific binding of IL-23 to the materials used in the study. Based on this data, it was assumed that the actual dose provided to monkeys was 16 ng/animal.

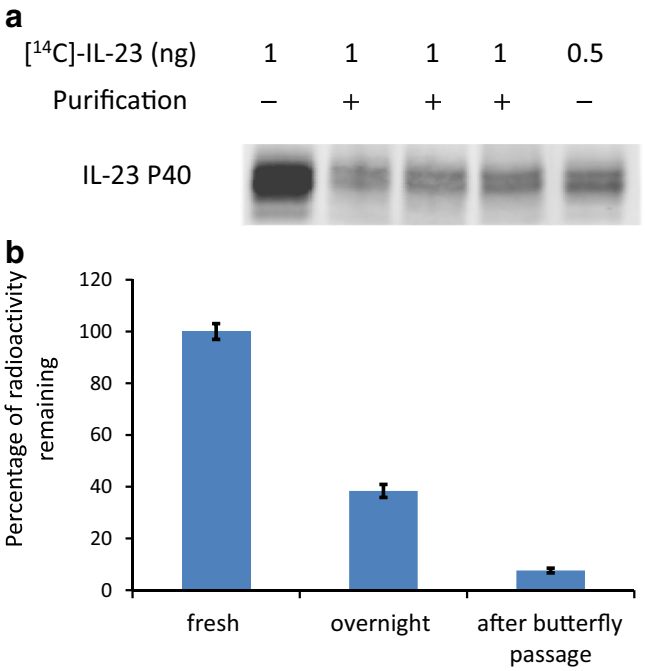


**Fig. 3.** Recovery of IL-23 after affinity purification, storage, and passage through dosing device. **a** The recovery of IL-23 after enrichment purification illustrated in western blot. Samples in the first and last lanes were prepared by directly loading 1 ng or 0.5 ng of [$^{14}$C]-IL-23 into western blot–loading buffer. Samples in other 3 lanes were prepared by spiking 1.4 mL of monkey serum with 1 ng of [$^{14}$C]-IL-23 prior to the immunoaffinity enrichment step. **b** The LSC measured the loss of radioactivity from mock dosing solution during storage and passage through a syringe

### [$^{14}$C]-IL-23 Pharmacokinetics in Cynomolgus Monkeys

The [$^{14}$C]-IL-23 concentration *vs* time profiles were slightly biphasic and similar among the 3 monkeys (Fig. 4). The mean clearance and volume of distribution at steady-state ($V_{ss}$) were 0.352 L/h and 1.43 L in monkey, respectively (Table I). The half-life of IL-23 was 4.8 h.

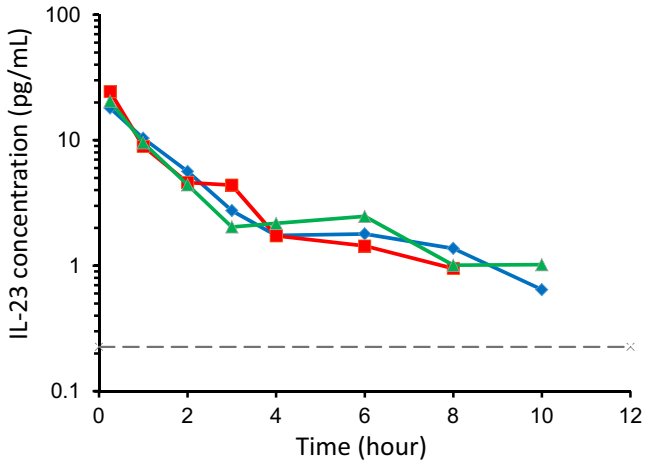


**Fig. 4.** Monkey [$^{14}$C]-IL-23 serum concentration *vs* time profile for 3 monkeys dosed intravenously with [$^{14}$C]-labeled human recombinant IL-23. The dashed line represents LLOQ. The nominal dose was 200 ng per animal, while the actual dose was 16 ng per animal after accounting for the non-specific binding loss

### Predicted Suppression of Free IL-23 by Anti-IL-23 Antibodies in Psoriasis

Free IL-23 suppression was simulated for the IL-23 monoclonal antibodies ustekinumab, tildrakizumab, guselkumab, and risankizumab using IL-23 clearance (3.32 L/h) and the volume of distribution (20 L) extrapolated allometrically from monkey data with exponents of 0.85 for clearance and 1.0 for volume of distribution (Table II) (49). Clinical efficacious dose levels used in the model were subcutaneous (SC) administration of 90 mg for ustekinumab, 200 mg for tildrakizumab, and 150 mg for risankizumab at 0, 4, and every 12 weeks thereafter; and 100 mg for guselkumab at 0, 4, and every 8 weeks thereafter.

The simulated systemic concentration of free IL-23 dropped to ≤ 10% of initial baseline following the first dose of antibodies (Fig. 5a). Free IL-23 levels remained deeply suppressed through drug trough concentration level ($C_{trough}$) for risankizumab and guselkumab dosing regimens (< 10% of initial baseline). In contrast, free IL-23 levels returned to near base levels at tildrakizumab and ustekinumab $C_{trough}$ (73% and 93%, respectively). The overall simulated reduction of free IL-23 by ustekinumab was within a comparable range to a recently published simulation (58). It is worth noting the reported baseline level of serum IL-23 varies, from 79 pg/mL in RA (50), 133 pg/mL in psoriasis (51), 179 pg/mL in moderate psoriasis, 191 pg/mL in severe psoriasis (6), and 408 pg/mL in Crohn's disease patients with skin lesions, during anti-TNF-α therapy (52). In the current work, the serum level of IL-23 in psoriasis was assumed to be 100 pg/mL; however, a similar level of IL-23 neutralization was predicted with assumed baseline concentrations 3-fold higher or lower for IL-23 (data not shown).

Risankizumab and guselkumab dosing regimens were predicted to have deeper and more sustained suppression of free IL-23 compared with ustekinumab and tildrakizumab dose regimens, predominantly due to greater affinity to IL-23 giving similarity among PK, doses, and dose frequency. The ranking of the area under the curve of the predicted percentage of free IL-23 from weeks 0 to 16 were ustekinumab > tildrakizumab > guselkumab > risankizumab (Fig. 5b), which aligned well with the observed efficacy (PASI 100 score) of these mAbs in clinical trials in psoriatic patients (Fig. 5c).

## DISCUSSION

Pro-inflammatory cytokines such as TNF-α, IL-1, IL-17, and IL-23 have been widely studied and targeted for the treatment of various diseases in the last three decades. Specifically, anti-IL-23 drugs have been tested for the treatment of several conditions, including psoriasis. Despite the clinical success of anti-IL23 antibodies for the treatment of psoriasis, quantitative information of IL-23 synthesis and clearance rates is largely absent in the literature due to challenges associated with quantifying the low levels of IL-23 *in vivo*. In this study, this inherent difficulty was overcome by

**Table I.** Pharmacokinetic parameters of [$^{14}$C]-IL-23 in monkey

| Subject No. | $t_{1/2}$ (h) | $C_{max}$ (pg/mL) | AUC (pg h/mL) | CL (L/h) | $V_{ss}$ (L) |
|---|---|---|---|---|---|
| 1 | 4.3 | 18.1 | 42.8 | 0.374 | 1.36 |
| 2 | 5.6 | 20.5 | 47.8 | 0.334 | 1.70 |
| 3 | 4.6 | 24.4 | 46.1 | 0.347 | 1.22 |
| Mean | 4.8 | 21.0 | 45.5 | 0.352 | 1.43 |
| SD | 0.7 | 3.2 | 2.6 | 0.020 | 0.25 |

utilizing AMS as a highly sensitive method to track the disappearance of a radiolabeled variant of the cytokine.

Human recombinant IL-23 was radiolabeled with [$^{14}$C] and intravenously injected into three monkeys. Cynomolgus monkey was selected as a model to explore the human recombinant IL-23 kinetics due to the accessibility of the animals and the high homology between human and monkey IL-23. To avoid the saturation of clearance mechanisms, the dose of [$^{14}$C]-IL-23 was designed to have a $C_{max}$ of < 20% of endogenous IL-23 levels. Two dose levels (400 pg and 200 ng/subject) were originally chosen because there is a wide range of published human serum IL-23 levels and our internal measured monkey IL-23 levels were 0.5–1 pg/mL (Singulex, Alameda, CA, Singulex Erenna human IL-23 immunoassay kit, cat# 03-0112-00) (data not shown).

Unexpectedly, initial AMS results indicated much lower blood concentrations than anticipated with [$^{14}$C]-IL-23 levels only detectable in monkeys in the 200 ng dose group. Additional follow-up experiments indicated a significant loss of the labeled cytokine prior to dosing (92.4% loss) due to non-specific binding to glass formulation vials and dosing syringes. Observed [$^{14}$C]-IL-23 blood concentrations were aligned with expectations after accounting for loss prior to dosing. Loss due to non-specific binding at such low levels of protein is not unique to IL-23, as similar issues have been observed for a vascular endothelial growth factor (VEGF) (internal data not shown). In response to this finding, an immunoaffinity enrichment step was added to enrich the specific [$^{14}$C]-IL-23 signal from endogenous [$^{14}$C] background levels prior to AMS analysis. Additionally, a standard curve was prepared to quantify the loss of the analyte upon handling. Future studies should be performed with the same controls to quantify the non-specific loss.

The calculated monkey IL-23 clearance and $V_{ss}$ were 0.352 L/h and 1.43 L, respectively. Via allometric scaling, the human IL-23 $V_{ss}$ was calculated as 20 L, which was comparable with IL-21 (26 L), but higher than reported values of IL-10 (4.9 L), IL-12 (~ 3–5 L), and IL-2 (7.9 L). The projected IL-23 clearance (3.32 L/h) was similar to IL-10 (3.35–4.1 L/h) in healthy volunteers (HV) but higher than published clearance of IL-12 (~ 0.5 L/h) in patients with advanced malignancies and lower than IL-2 (7 L/h) in HV and IL-21 (15 L/h) in patients with metastatic melanoma (10–13), possibly due to the size differences between IL-12 (75 kDa), IL-23 (53 kDa), IL-10 (21 kDa), IL-2 (15 kDa), and IL-21(15 kDa). However, the disease conditions and high dose levels used in IL-2 and IL-21 studies could also impact clearance readouts and warrants further investigation.

IL-23 kinetics measured in this study enabled the establishment of a ligand-binding PK/PD model to predict free IL-23 suppression by anti-IL-23 drugs. A ligand-binding PK/PD model was derived from the target-mediated drug disposition (TMDD) model, which was first proposed in 2001 by Mager and Jusko (36), and underwent extensive refinement in subsequent reports (39,59–61). This model has been applied in numerous studies ranging from works in early discovery to the late development stages of drug development

**Table II.** Parameters used in ligand-binding model for risankizumab, tildrakizumab, guselkumab, and ustekinumab in psoriasis clinical trials

| | Parameter | Value | | | |
|---|---|---|---|---|---|
| IL-23 | $C_{ss}$ (pg/mL)[a] | 100 | | | |
| | $k_{syn}$ (nM/h) | 0.000313 | | | |
| | $k_{deg}$ (/h) | 0.166 | | | |
| | $V$ (L) | 20 | | | |
| | | Risankizumab (42,43) | Ustekinumab (44,45) | Guselkumab (46) | Tildrakizumab (47,48) |
| Antibody | $V$ (L) | 9.09 | 8.95 | 7.2 | 5.69 |
| | $k_{10}$ (/h) | 0.00138 | 0.00123 | 0.00185 | 0.0011 |
| | $k_a$ (/h) | 0.0075 | 0.0148 | 0.013 | 0.0071 |
| | $F$% (SC) | 72 | 57 | 40 | 92 |
| | $K_D$ (nM)[b] | 0.002 | 0.079 | 0.0033[c] | 0.3 |

[a] Baseline serum concentration at steady-state without treatment
[b] Published lowest $K_D$ or *in vitro* $IC_{50}$
[c] From FDA BLA document
*SC* subcutaneous

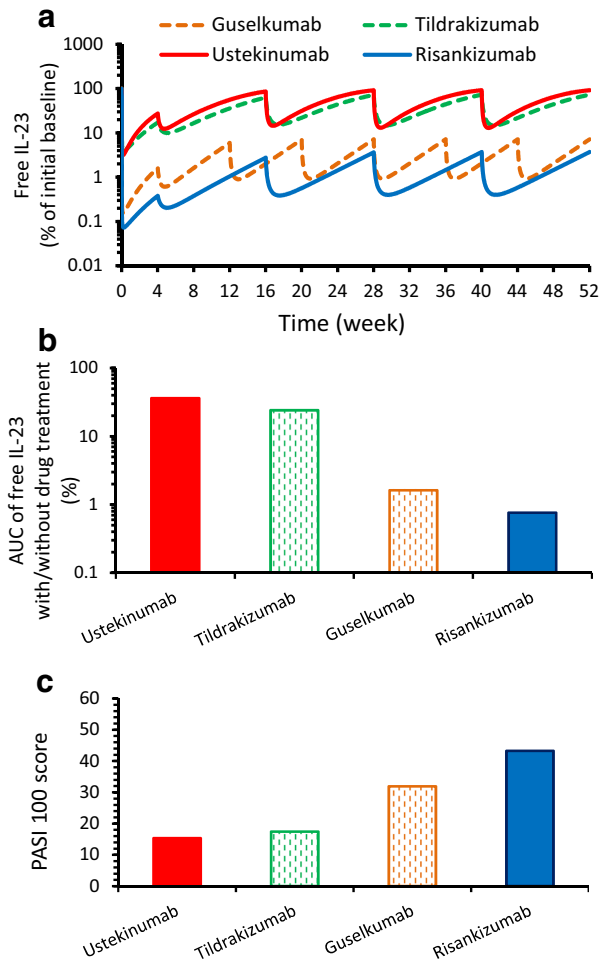


**Fig. 5.** Simulated free IL-23 in blood and comparison with PASI 100 scores reported in psoriasis clinical trials. **a** Predicted free IL-23, expressed as % of initial baseline in blood following ustekinumab, tildrakizumab, guselkumab, and risankizumab treatments. **b** Area under the curves of predicted free IL-23 from week 0 to 16 follows ustekinumab, tildrakizumab, guselkumab, and risankizumab treatments expressed as % of no treatment control. **c** Bar graph plotted with published PASI 100 scores for treatment with ustekinumab, tildrakizumab, guselkumab, and risankizumab in psoriasis. The baseline serum level of IL-23 is assumed as 100 pg/mL in psoriasis patients based on the range of serum IL-23 levels reported in patients with autoimmune diseases (6,50–52). Clinical efficacious dose levels via subcutaneous (SC) administration were 90 mg for ustekinumab, 200 mg for tildrakizumab, and 150 mg for risankizumab at 0, 4, and every 12 weeks thereafter; and 100 mg for guselkumab at 0, 4, and every 8 weeks thereafter. The percentage of free IL-23 was calculated as simulated free IL-23 divided by the baseline level of IL-23 and multiplied by 100. Reported PASI 100 score was read at 12 weeks after dose for ustekinumab (average result from PHOENIX 1 and 2 trials) (53–55) and tildrakizumab (reSURFACE 1 and 2 trials) (56), 16 weeks after dose for risankizumab (average of IMMvent, IMMhance, UltIMMa-1, and UltIMMa-2 trials) from publicly released data from AbbVie, and guselkumab in VOYAGE 1 and 2 trials (57)

(62,63). A PK/PD model for free IL-23 suppression is of significant interest due to the limited and sometimes inconsistent IL-23 readouts of downstream mechanistic biomarkers (42,64,65). The accurate measurement of free as target-engagement biomarkers is challenging due to their low levels and the interference of anti-IL-23 drugs. Moreover, mechanistic biomarkers, which could be a potential surrogate for target coverage, have not been identified and confirmed. Therefore, modeling and simulation of IL-23 coverage may provide needed quantitative data to help decision making with regard to ranking the efficacy of anti-IL-23 antibodies and selecting doses and dose regimens.

In the current simulation, free IL-23 suppression was predicted for the IL-23 monoclonal antibodies ustekinumab, tildrakizumab, guselkumab, and risankizumab. While the last 3 mAbs specifically inhibit the unique p19 subunit of IL-23, ustekinumab targets the p40 subunit of IL-23 which is shared with IL-12. However, previously published data suggested IL-12 is less critical than IL23 in the development of psoriasis and the suppression of IL-23 by ustekinumab appears to be the main driving force of its efficacy and thus is the focus of the current simulation (51,66–69).

As shown in the current work, free serum IL-23 levels after treatment with anti- IL-23 mAbs ustekinumab, tildrakizumab, guselkumab, or risankizumab were simulated and the results were compared with the efficacy endpoint PASI 100 scores from clinical trials for the treatment of psoriasis. Despite the alignment between predicted IL-23 suppressions and PASI 100 scores, limitations in this simulation are recognized. For example, the elimination rate of IL-23-antibody complexes was assumed to be the same as that of the antibody. In addition, systemic IL-23 suppressions were predicted as the surrogate indicators of target tissue IL-23 inhibition and assuming the ranking order of anti-IL-23 efficacy in tissues is the same as in blood for four drugs. It is possible that the percentage of IL-23 coverage in target tissue skin is lower than that in the blood considering the higher local IL-23 expression and the lower tissue distribution of antibodies (70). Adding complexity on projecting local IL-23 suppression, the clearance of local IL-23 and IL-23-antibody complexes may impact the local IL-23 neutralization efficacy and warrants further investigation. Nevertheless, the correlation between simulated free IL-23 suppression in blood and efficacy of the anti-IL-23 antibodies demonstrates that a PK/PD modeling approach is valid and could be potentially used to predict the efficacy for anti-IL23 drugs in clinical trials. It is also worth mentioning that the predicted suppression of IL-23 correlated with efficacy, but not safety as demonstrated by similar adverse effects of interest across phase 3 trials (56,71,72).

In another recent publication, IL-23 suppression by ustekinumab was predicted with a minimal physiologically based pharmacokinetic (mPBPK) model (58). In the paper, Chen quantitatively assessed the kinetics and interrelationship between a monoclonal anti-IL-23 antibody CNTO 3723 and an exogenously administered recombinant mouse IL-23 (rmIL-23) in both serum and lesional skin sites of mice. The estimated clearance and half-life of rmIL-23 in mice were 307 mL/day and 3 min, respectively. These values, after allometric scaling to the monkey, are significantly different from rhIL-23 measures reported here. The higher clearance and shorter half-life reported by Chen may reflect different IL-23 kinetics between two species and/or the sensitivity of the different detection methods used and the different dose levels tested. To understand the impact of different parameter inputs on the prediction

of free IL-23 suppression, we simulated IL-23 suppression with the two main parameters from Chen's paper via the simple ligand-binding model used in the current work. Incorporating Chen's higher (10×) degradation rate of IL-23 ($k_{deg}$) and higher (5×) elimination rate of the IL-23-drug complex ($k_{el}$) into the current model led to a similar predicted free IL-23 suppression as reported by Chen, possibly due to the offset effects of two parameters (data not shown). Nevertheless, the overall prediction of free IL-23 inhibitions by ustekinumab was comparable in our work and Chen's despite the discrepancy of some parameter inputs and the use of different models.

## CONCLUSION

In conclusion, we have utilized highly sensitive AMS to measure rhIL23 PK parameters in monkey, including clearance and volume of distribution. This report is the first example of these values being measured with the administration of IL-23 at exposure levels similar to that of the endogenous cytokine. This data enabled the development of a model used to predict suppression of free IL-23 by four therapeutic mAbs. The results of these simulations showed good correlation with the reported efficacy of the four drugs, suggesting that the strategy used herein may be useful to predict efficacious doses of therapeutic mAbs against other soluble targets.

## ACKNOWLEDGMENTS

The authors would like to thank Xceleron for the AMS measurements and helpful discussions. The authors wish to thank Jeff Barbon and Meha Chhaya from AbbVie Bioresearch Center (ABC) for providing the HeLa bioassay and guidance on study design, Yu Tian and Kim Youngjae from ABC for bioanalytical support, Yuni Fang and Vivian V. Zhao from AbbVie Redwood City for providing the IL-23 level in monkeys and healthy volunteers, and Colin J. Phipps from AbbVie for the review of modeling and helpful discussions. Finally, we gratefully acknowledge Candace Graff and Melanie C. Ruzek for their critical review of the manuscript.

## FUNDING INFORMATION

AbbVie provided funding for AMS analysis by the contract lab Xceleron (Pharmaron).

## COMPLIANCE WITH ETHICAL STANDARDS

**Conflict of Interest** Junli Ma, Timothy Montavon, Susan E. Lacy, Gary J. Jenkins, Stella Doktor, and J. Cory Kalvass are employees of AbbVie. Kenneth R. Durbin is a former AbbVie employee and is now an employee of Proteinaceous Inc., and has no other conflict of interest to disclose. Ting-Ting Zhang is a former AbbVie employee and is now an employee of Takeda Pharmaceuticals International Co., and has no other conflict of interest to disclose. All authors may own AbbVie stock. AbbVie sponsored and funded the study; contributed to the design; participated in the collection, analysis, and interpretation of data, and in writing, reviewing, and approval of the final publication.

## REFERENCES

1. Szollosi DE, et al. Current and novel anti-inflammatory drug targets for inhibition of cytokines and leucocyte recruitment in rheumatic diseases. J Pharm Pharmacol. 2017.
2. Mizuma A, Yenari MA. Anti-inflammatory targets for the treatment of reperfusion injury in stroke. Front Neurol. 2017;8:467.
3. Krebs CF, Schmidt T, Riedel JH, Panzer U. T helper type 17 cells in immune-mediated glomerular disease. Nat Rev Nephrol. 2017;13(10):647–59.
4. Yago T, et al. IL-23 and Th17 disease in inflammatory arthritis. J Clin Med. 2017;6:9.
5. Sadeghi M, et al. IL-23 plasma level is strongly associated with CMV status and reactivation of CMV in renal transplant recipients. BMC Immunol. 2016;17(1):35.
6. Wang XY, Chen XY, Li J, Zhang HY, Liu J, Sun LD. MiR-200a expression in CD4+ T cells correlates with the expression of Th17/Treg cells and relevant cytokines in psoriasis vulgaris: a case control study. Biomed Pharmacother. 2017;93:1158–64.
7. Lee JW, Kelley M, King LE, Yang J, Salimi-Moosavi H, Tang MT, et al. Bioanalytical approaches to quantify "total" and "free" therapeutic antibodies and their targets: technical challenges and PK/PD applications over the course of drug development. AAPS J. 2011;13(1):99–110.
8. Wang W, Wang X, Doddareddy R, Fink D, McIntosh T, Davis HM, et al. Mechanistic pharmacokinetic/target engagement/pharmacodynamic (PK/TE/PD) modeling in deciphering interplay between a monoclonal antibody and its soluble target in cynomolgus monkeys. AAPS J. 2014;16(1):129–39.
9. Hu L, Hansen RJ. Issues, challenges, and opportunities in model-based drug development for monoclonal antibodies. J Pharm Sci. 2013;102(9):2898–908.
10. Huhn RD, et al. Pharmacokinetics and immunomodulatory properties of intravenously administered recombinant human interleukin-10 in healthy volunteers. Blood. 1996;87(2):699–705.
11. Davis ID, Skrumsager BK, Cebon J, Nicholaou T, Barlow JW, Moller NPH, et al. An open-label, two-arm, phase I trial of recombinant human interleukin-21 in patients with metastatic melanoma. Clin Cancer Res. 2007;13(12):3630–6.
12. Konrad MW, Hemstreet G, Hersh EM, Mansell PW, Mertelsmann R, Kolitz JE, et al. Pharmacokinetics of recombinant interleukin 2 in humans. Cancer Res. 1990;50(7):2009–17.
13. Atkins MB, et al. Phase I evaluation of intravenous recombinant human interleukin 12 in patients with advanced malignancies. Clin Cancer Res. 1997;3(3):409–17.
14. Creaven PJ, et al. Phase I clinical trial of recombinant human tumor necrosis factor. Cancer Chemother Pharmacol. 1987;20(2):137–44.
15. Gamm H, Lindemann A, Mertelsmann R, Herrmann F. Phase I trial of recombinant human tumour necrosis factor alpha in patients with advanced malignancy. Eur J Cancer. 1991;27(7):856–63.
16. Castell JV, et al. Plasma clearance, organ distribution and target cells of interleukin-6/hepatocyte-stimulating factor in the rat. Eur J Biochem. 1988;177(2):357–61.
17. Kudo S, et al. Clearance and tissue distribution of recombinant human interleukin 1 beta in rats. Cancer Res. 1990;50(18):5751–5.
18. Gibbons JA, Luo ZP, Hannon ER, Braeckman RA, Young JD. Quantitation of the renal clearance of interleukin-2 using nephrectomized and ureter-ligated rats. J Pharmacol Exp Ther. 1995;272(1):119–25.
19. Vlaming ML, et al. Microdosing of a carbon-14 labeled protein in healthy volunteers accurately predicts its pharmacokinetics at therapeutic dosages. Clin Pharmacol Ther. 2015;98(2):196–204.
20. Hunter CA. New IL-12-family members: IL-23 and IL-27, cytokines with divergent functions. Nat Rev Immunol. 2005;5(7):521–31.
21. Oppmann B, Lesley R, Blom B, Timans JC, Xu Y, Hunte B, et al. Novel p19 protein engages IL-12p40 to form a cytokine,

IL-23, with biological activities similar as well as distinct from IL-12. Immunity. 2000;13(5):715–25.
22. Parham C, Chirica M, Timans J, Vaisberg E, Travis M, Cheung J, et al. A receptor for the heterodimeric cytokine IL-23 is composed of IL-12Rbeta1 and a novel cytokine receptor subunit, IL-23R. J Immunol. 2002;168(11):5699–708.
23. Piskin G, Sylva-Steenland RMR, Bos JD, Teunissen MBM. In vitro and in situ expression of IL-23 by keratinocytes in healthy skin and psoriasis lesions: enhanced expression in psoriatic skin. J Immunol. 2006;176(3):1908–15.
24. McKenzie BS, Kastelein RA, Cua DJ. Understanding the IL-23-IL-17 immune pathway. Trends Immunol. 2006;27(1):17–23.
25. Liu W, Ouyang X, Yang J, Liu J, Li Q, Gu Y, et al. AP-1 activated by toll-like receptors regulates expression of IL-23 p19. J Biol Chem. 2009;284(36):24006–16.
26. Volpe E, et al. Thymic stromal lymphopoietin links keratinocytes and dendritic cell-derived IL-23 in patients with psoriasis. J Allergy Clin Immunol. 2014;134(2):373–81.
27. Wang Q, Franks HA, Porte J, el Refaee M, Shah S, Crooks J, et al. Novel approach for interleukin-23 up-regulation in human dendritic cells and the impact on T helper type 17 generation. Immunology. 2011;134(1):60–72.
28. Mangan PR, Harrington LE, O'Quinn DB, Helms WS, Bullard DC, Elson CO, et al. Transforming growth factor-beta induces development of the T(H)17 lineage. Nature. 2006;441(7090):231–4.
29. Ivanov II, et al. The orphan nuclear receptor RORgammat directs the differentiation program of proinflammatory IL-17+ T helper cells. Cell. 2006;126(6):1121–33.
30. El-Behi M, et al. The encephalitogenicity of T(H)17 cells is dependent on IL-1- and IL-23-induced production of the cytokine GM-CSF. Nat Immunol. 2011;12(6):568–75.
31. Codarri L, Gyülvészi G, Tosevski V, Hesske L, Fontana A, Magnenat L, et al. RORgammat drives production of the cytokine GM-CSF in helper T cells, which is essential for the effector phase of autoimmune neuroinflammation. Nat Immunol. 2011;12(6):560–7.
32. Gaffen SL, Jain R, Garg AV, Cua DJ. The IL-23-IL-17 immune axis: from mechanisms to therapeutic testing. Nat Rev Immunol. 2014;14(9):585–600.
33. Langrish CL, Chen Y, Blumenschein WM, Mattson J, Basham B, Sedgwick JD, et al. IL-23 drives a pathogenic T cell population that induces autoimmune inflammation. J Exp Med. 2005;201(2):233–40.
34. Frieder J, et al. Anti-IL-23 and anti-IL-17 biologic agents for the treatment of immune-mediated inflammatory conditions. Clin Pharmacol Ther. 2017.
35. Campa M, Mansouri B, Warren R, Menter A. A review of biologic therapies targeting IL-23 and IL-17 for use in moderate-to-severe plaque psoriasis. Dermatol Ther (Heidelb). 2016;6(1):1–12.
36. Mager DE, Jusko WJ. General pharmacokinetic model for drugs exhibiting target-mediated drug disposition. J Pharmacokinet Pharmacodyn. 2001;28(6):507–32.
37. Dua P, Hawkins E, van der Graaf PH. A tutorial on target-mediated drug disposition (TMDD) models. CPT Pharmacometrics Syst Pharmacol. 2015;4(6):324–37.
38. Soman A, Qiu Y, Chan Li Q. HPLC-UV method development and validation for the determination of low level formaldehyde in a drug substance. J Chromatogr Sci. 2008;46(6):461–5.
39. Mager DE, Krzyzanski W. Quasi-equilibrium pharmacokinetic model for drugs exhibiting target-mediated drug disposition. Pharm Res. 2005;22(10):1589–96.
40. Tiwari A, Kasaian M, Heatherington AC, Jones HM, Hua F. A mechanistic PK/PD model for two anti-IL13 antibodies explains the difference in total IL-13 accumulation observed in clinical studies. MAbs. 2016;8(5):983–90.
41. Lupardus PJ, Garcia KC. The structure of interleukin-23 reveals the molecular basis of p40 subunit sharing with interleukin-12. J Mol Biol. 2008;382(4):931–41.
42. Krueger JG, Ferris LK, Menter A, Wagner F, White A, Visvanathan S, et al. Anti-IL-23A mAb BI 655066 for treatment of moderate-to-severe psoriasis: safety, efficacy, pharmacokinetics, and biomarker results of a single-rising-dose, randomized, double-blind, placebo-controlled trial. J Allergy Clin Immunol. 2015;136(1):116–124 e7.
43. Suleiman AA, et al. Population pharmacokinetics of the Interleukin-23 inhibitor risankizumab in subjects with psoriasis and Crohn's disease: analyses of phase I and II trials. Clin Pharmacokinet. 2018.
44. Zhu Y, Hu C, Lu M, Liao S, Marini JC, Yohrling J, et al. Population pharmacokinetic modeling of ustekinumab, a human monoclonal antibody targeting IL-12/23p40, in patients with moderate to severe plaque psoriasis. J Clin Pharmacol. 2009;49(2):162–75.
45. Li J, Wei H, Krystek SR Jr, Bond D, Brender TM, Cohen D, et al. Mapping the energetic epitope of an antibody/interleukin-23 interaction with hydrogen/deuterium exchange, fast photochemical oxidation of proteins mass spectrometry, and alanine shave mutagenesis. Anal Chem. 2017;89(4):2250–8.
46. Zhuang Y, Calderon C, Marciniak SJ, Bouman-Thio E, Szapary P, Yang TY, et al. First-in-human study to assess guselkumab (anti-IL-23 mAb) pharmacokinetics/safety in healthy subjects and patients with moderate-to-severe psoriasis. Eur J Clin Pharmacol. 2016;72(11):1303–10.
47. Zandvliet A, et al. Tildrakizumab, a novel anti-IL-23 monoclonal antibody, is unaffected by ethnic variability in Caucasian, Chinese, and Japanese subjects. Int J Clin Pharmacol Ther. 2015;53(2):139–46.
48. Kopp T, et al. Clinical improvement in psoriasis with specific targeting of interleukin-23. Nature. 2015;521(7551):222–6.
49. Deng R, Iyer S, Theil FP, Mortensen DL, Fielder PJ, Prabhu S. Projecting human pharmacokinetics of therapeutic antibodies from nonclinical data: what have we learned? MAbs. 2011;3(1):61–6.
50. Zaky DS, El-Nahrery EM. Role of interleukin-23 as a biomarker in rheumatoid arthritis patients and its correlation with disease activity. Int Immunopharmacol. 2016;31:105–8.
51. Brito-Luna MJ, Villanueva-Quintero DG, Sandoval-Talamantes AK, Fafutis-Morris M, Graciano-Machuca O, Sanchez-Hernandez PE, et al. Correlation of IL-12, IL-22, and IL-23 in patients with psoriasis and metabolic syndrome. Preliminary report. Cytokine. 2016;85:130–6.
52. Wlodarczyk M, et al. Correlations between skin lesions induced by anti-tumor necrosis factor-alpha and selected cytokines in Crohn's disease patients. World J Gastroenterol. 2014;20(22):7019–26.
53. Rich P, Bourcier M, Sofen H, Fakharzadeh S, Wasfi Y, Wang Y, et al. Ustekinumab improves nail disease in patients with moderate-to-severe psoriasis: results from PHOENIX 1. Br J Dermatol. 2014;170(2):398–407.
54. Leonardi CL, Kimball AB, Papp KA, Yeilding N, Guzzo C, Wang Y, et al. Efficacy and safety of ustekinumab, a human interleukin-12/23 monoclonal antibody, in patients with psoriasis: 76-week results from a randomised, double-blind, placebo-controlled trial (PHOENIX 1). Lancet. 2008;371(9625):1665–74.
55. Papp KA, Langley RG, Lebwohl M, Krueger GG, Szapary P, Yeilding N, et al. Efficacy and safety of ustekinumab, a human interleukin-12/23 monoclonal antibody, in patients with psoriasis: 52-week results from a randomised, double-blind, placebo-controlled trial (PHOENIX 2). Lancet. 2008;371(9625):1675–84.
56. Reich K, Papp KA, Blauvelt A, Tyring SK, Sinclair R, Thaçi D, et al. Tildrakizumab versus placebo or etanercept for chronic plaque psoriasis (reSURFACE 1 and reSURFACE 2): results from two randomised controlled, phase 3 trials. Lancet. 2017;390(10091):276–88.
57. Blauvelt A, et al. Efficacy and safety of guselkumab, an anti-interleukin-23 monoclonal antibody, compared with adalimumab for the continuous treatment of patients with moderate to severe psoriasis: results from the phase III, double-blinded, placebo- and active comparator-controlled VOYAGE 1 trial. J Am Acad Dermatol. 2017;76(3):405–17.
58. Chen X, Jiang X, Doddareddy R, Geist B, McIntosh T, Jusko WJ, et al. Development and translational application of a minimal physiologically based pharmacokinetic model for a monoclonal antibody against interleukin 23 (IL-23) in IL-23-induced psoriasis-like mice. J Pharmacol Exp Ther. 2018;365(1):140–55.

59. Gibiansky L, Gibiansky E. Target-mediated drug disposition model: approximations, identifiability of model parameters and applications to the population pharmacokinetic-pharmacodynamic modeling of biologics. Expert Opin Drug Metab Toxicol. 2009;5(7):803–12.
60. Gibiansky L, Gibiansky E, Kakkar T, Ma P. Approximations of the target-mediated drug disposition model and identifiability of model parameters. J Pharmacokinet Pharmacodyn. 2008;35(5):573–91.
61. Davda JP, Hansen RJ. Properties of a general PK/PD model of antibody-ligand interactions for therapeutic antibodies that bind to soluble endogenous targets. MAbs. 2010;2(5):576–88.
62. Agoram BM, Martin SW, van der Graaf PH. The role of mechanism-based pharmacokinetic-pharmacodynamic (PK-PD) modelling in translational research of biologics. Drug Discov Today. 2007;12(23–24):1018–24.
63. Aston PJ, Derks G, Raji A, Agoram BM, van der Graaf PH. Mathematical analysis of the pharmacokinetic-pharmacodynamic (PKPD) behaviour of monoclonal antibodies: predicting in vivo potency. J Theor Biol. 2011;281(1):113–21.
64. Mannon PJ, Fuss IJ, Mayer L, Elson CO, Sandborn WJ, Present D, et al. Anti-interleukin-12 antibody for active Crohn's disease. N Engl J Med. 2004;351(20):2069–79.
65. Sofen H, Smith S, Matheson RT, Leonardi CL, Calderon C, Brodmerkel C, et al. Guselkumab (an IL-23-specific mAb) demonstrates clinical and molecular response in patients with moderate-to-severe psoriasis. J Allergy Clin Immunol. 2014;133(4):1032–40.
66. Lee E, Trepicchio WL, Oestreicher JL, Pittman D, Wang F, Chamian F, et al. Increased expression of interleukin 23 p19 and p40 in lesional skin of patients with psoriasis vulgaris. J Exp Med. 2004;199(1):125–30.
67. Toichi E, Torres G, McCormick TS, Chang T, Mascelli MA, Kauffman CL, et al. An anti-IL-12p40 antibody down-regulates type 1 cytokines, chemokines, and IL-12/IL-23 in psoriasis. J Immunol. 2006;177(7):4917–26.
68. Torres T. Selective Interleukin-23 p19 inhibition: another game changer in psoriasis? Focus on risankizumab. Drugs. 2017;77(14):1493–503.
69. Ogawa K, Matsumoto T, Esaki M, Torisu T, Iida M. Profiles of circulating cytokines in patients with Crohn's disease under maintenance therapy with infliximab. J Crohns Colitis. 2012;6(5):529–35.
70. Shah DK, Betts AM. Antibody biodistribution coefficients: inferring tissue concentrations of monoclonal antibodies based on the plasma concentrations in several preclinical species and human. MAbs. 2013;5(2):297–305.
71. Gordon KB, Strober B, Lebwohl M, Augustin M, Blauvelt A, Poulin Y, et al. Efficacy and safety of risankizumab in moderate-to-severe plaque psoriasis (UltIMMa-1 and UltIMMa-2): results from two double-blind, randomised, placebo-controlled and ustekinumab-controlled phase 3 trials. Lancet. 2018;392(10148):650–61.
72. Langley RG, Tsai TF, Flavin S, Song M, Randazzo B, Wasfi Y, et al. Efficacy and safety of guselkumab in patients with psoriasis who have an inadequate response to ustekinumab: results of the randomized, double-blind, phase III NAVIGATE trial. Br J Dermatol. 2018;178(1):114–23.